Journal of Power Sources 196 (2011) 4095–4101

Contents lists available at ScienceDirect

Journal of Power Sources

journal homepage: www.elsevier.com/locate/jpowsour

Dual functions of activated carbon in a positive electrode for MnO_2-based hybrid supercapacitor

Peng-Cheng Gao, An-Hui Lu, Wen-Cui Li*

State Key Laboratory of Fine Chemicals, School of Chemical Engineering, Dalian University of Technology, Dalian 116012, China

ARTICLE INFO

Article history:
Received 16 August 2010
Received in revised form
11 November 2010
Accepted 16 December 2010
Available online 23 December 2010

Keywords:
Hybrid supercapacitor
Aqueous electrolyte
Positive electrode
Activated carbon
Manganese dioxide

ABSTRACT

Utilizing the dual functions of activated carbon (AC) both as a conductive agent and an active substance of a positive electrode, a hybrid supercapacitor (AC-MnO_2&AC) with a composite of manganese dioxide (MnO_2) and activated carbon as the positive electrode (MnO_2&AC) and AC as the negative electrode is fabricated, which integrates approximate symmetric and asymmetric behaviors in the distinct parts of 2 V operating windows. MnO_2 in the positive electrode and AC in the negative electrode together form a pure asymmetric structure, which extends the operating voltage to 2 V due to the compensatory effect of opposite over-potentials. In the range of 0–1.1 V, both AC in the positive and negative electrode assemble as a symmetric structure via a parallel connection which offers more capacitance and less internal resistance. The optimal mass proportions of electrodes are calculated though a mathematical process. In a stable operating window of 2 V, the capacitance of AC-MnO_2&AC can reach 33.2 F g^{-1}. After 2500 cycles, maximum energy density is 18.2 Wh kg^{-1} with a 4% loss compared to the initial cycle. The power density is 10.1 kW kg^{-1} with an 8% loss.

1. Introduction

Supercapacitors (SC) with attractive characteristics such as high power density, low equivalent series resistance (ESR) and permanent charge–discharge life are considered as promising energy storage devices that perfectly fill the gap between dielectric capacitors and traditional batteries [1]. In the light of green chemistry and cost reduction, high energy density SC based on aqueous electrolyte is more desirable. The amount of electrical energy (E) accumulated in SC is proportional to the capacitance (C) and operating voltage (V), as shown in Eq. (1). Both broadening operating voltage and increasing the capacitance will be efficient strategies for the enhancement of energy density [2].

$$E = \frac{1}{2}CV^2 \quad (1)$$

An asymmetric configuration, where the relative electrodes are constituted from MnO_2 and activated carbon (AC) with opposite over-voltage, has recently been proved to be an effective model to extend the voltage window in aqueous systems [3]. Béguin et al. reported that an asymmetric SC using MnO_2 and activated carbon as positive and negative electrode, respectively, can be operated at 2 V in aqueous solution [4–6]. Long-term cycling stability of such asymmetric SC with capacitance of 23 F g^{-1} was achieved by removing dissolved oxygen from the electrolyte [7]. Besides manganese oxides [8,9], other metal oxides as positive materials and porous carbon material as negative materials have been investigated in the past years [10–13]. Among them, MnO_2 with attractive properties such as low cost and environment-friendly is considered as a promising electrode material. However, owing to its low electrical conductivity, MnO_2 electrode needs to be incorporated with acetylene black (AB) [14], carbon nanotubes [15,16] or conductive polymer [17]. Simon et al. demonstrated that excessive addition of conductive agent would result in a decrease in specific capacitance because of extra mass gain, other than improving the multiplying power [18]. With the aim to optimize the electrochemical behaviors of MnO_2, activated carbon was doped into MnO_2 via physical mixing [19], chemical or electrochemical deposition [20–22]. Compared with pure MnO_2 electrode, composite electrodes exhibit improved electrical conductivity. Moreover, it is possible to implant uniformly distributed pseudocapacitive species on carbon surfaces thus to exploit high energy [23–25]. Most of previous works on composite electrode focused on the discussion of capacitive behaviors of composite material and tested in a three-electrode system. However, in the working range of MnO_2 (usually from 0 V to 1.0 V in a three-electrode system), the used activated carbon usually enters into dormant state and offers negligible contribution to a capacitance. Hence, this activated carbon was only limited to be as conducting or structure supporting agent [21–25]. As a consequence, it has been neglected that activated carbon in a composite electrode might

* Corresponding author. Tel.: +86 411 3960 8206; fax: +86 411 3960 8206.
E-mail addresses: pengchenggao_dlut@yahoo.cn (P.-C. Gao), anhuilu@dlut.edu.cn (A.-H. Lu), wencuili@dlut.edu.cn (W.-C. Li).

0378-7753/$ – see front matter © 2010 Elsevier B.V. All rights reserved.
doi:10.1016/j.jpowsour.2010.12.056

take as one part of circuit and offer capacitance in a two-electrode system.

In the present work, we established a fabrication of hybrid supercapacitor based on using composite material (MnO_2&AC) as the positive electrode and AC as the negative electrode. Herein, AC used in the MnO_2&AC positive electrode not only functions as a conductive agent but also serves as an active substance of the positive electrode in an approximate symmetric system manner. Between 0 V and 1.1 V, AC in positive electrode works and provides the additional capacitance though the parallel connection with AC in negative electrode. This fabrication strategy is different from "pure" asymmetric system where carbon nanotube, activated carbon or polyaniline is used only for enhancing the conductivity.

2. Experimental

2.1. Preparation of electrode materials

MnO_2 powder was synthesized by a chemical precipitation method [14]. Briefly, 0.158 g $KMnO_4$ (99% purity) was dissolved in deionized water to obtain a 20 ml solution with a concentration of 0.05 M. Afterwards, 0.05 M $Mn(OAC)_2$ solution with 30 ml in volume was added drop-wise at the rate of 1 ml min^{-1} under stirring. This mixed solution was continuously stirred for 6 h. The precipitated sample was collected and thoroughly washed with deionized water, and then subject to drying at 110 °C for 12 h. Commercial AC (YP/47, Japan) was used for the preparation of both positive and negative electrodes.

2.2. Structure characterizations

The morphology of MnO_2 was examined using scanning electron microscope (SEM, Hitachi, S4800). Powder X-ray diffraction (XRD) pattern was recorded on a D/Max-2400 diffract meter utilizing a Cu Kα X-ray radiation, with a voltage of 45 kV and current of 40 mA. Nitrogen sorption measurement was carried out with a Micromeritics Tristar3000 adsorption analyzer at 77 K. Prior to adsorption experiment, the sample was degassed for 4 h at 120 °C. The specific surface areas (S_{BET}) were calculated from adsorption data in the relative pressure range of 0.05–0.3 by using the Brunauer–Emmett–Teller (BET) model. The pore size distribution of MnO_2 was evaluated using the Barret–Joyner–Halenda (BJH) method based on the desorption branch, whereas the pore size distribution of AC was evaluated by the density functional theory (DFT) model. The total pore volume was estimated from the amount adsorbed at a relative pressure of 0.90.

2.3. Electrochemical measurements

The composite positive electrodes (MnO_2&AC15) were prepared by mixing the MnO_2 powder with AC, acetylene black (AB) and polytetrafluoroethylene (PTFE) in a mass percentage of 70:15:10:5 through ultrasonic treatment. Here AB was used as the conductive agent and PTFE as binder.

The mixture was thoroughly homogenized in an agate mortar and dried at room temperature before being rolled into a uniform thin film. The electrodes were made by cutting this thin film into discs with surface area of ca. 1 cm^2, corresponding to a mass of approximately 6.5 mg. For comparison, two extra positive electrodes without using AC but with the same percentage of MnO_2 ($m_{MnO_2} : m_{AB} : m_{PTFE} = 70 : 25 : 5$) and the same percentage of AB ($m_{MnO_2} : m_{AB} : m_{PTFE} = 85 : 10 : 5$) were prepared, which were named as MnO_2&AB25 and MnO_2&AB10, respectively. To demonstrate the optimal mass of AC in positive electrode, series of composite electrode with varied mass of AC were prepared. The componential information of the positive electrodes used in this paper was listed in Table 1. AC negative electrodes were prepared only using a mixture of 85 wt.% commercial AC, 10 wt.% AB and 5 wt.% PTEF by the same technique.

Table 1
Components of the positive electrodes used.

Positive electrode	MnO_2 (%)	AC[a] (%)	AB[b] (%)	PTEF[c] (%)
MnO_2&AC7	78	7	10	5
MnO_2&AC15	70	15	10	5
MnO_2&AC25	60	25	10	5
MnO_2&AC35	50	35	10	5
MnO_2&AB10	85	–	10	5
MnO_2&AB25	70	–	25	5

[a] AC, activated carbon.
[b] AB, acetylene black.
[c] PTEF, polytetrafluoroethylene.

The electrochemical measurements were first done in Teflon three-electrode system in 0.5 M Na_2SO_4 aqueous solution using a stainless-steel grid as the current collector, meanwhile, using Pt and Hg/Hg_2SO_4 as the auxiliary and reference electrodes, respectively. Three-electrode tests were performed using CHI602C/606C from Chenhua Company. Two-electrode glass cell tests were performed using Arbin BT2000-10V-5A-8CH multi-channel college station. Before the electrochemical test, the pH value of the Na_2SO_4 aqueous solution was adjusted to 6.4 by adding H_2SO_4. The specific capacitances (C) of the electrodes in Farads per gram are calculated from the discharge curve based on Eq. (2).

$$C = \frac{I \times \Delta t}{\Delta V} \tag{2}$$

where I in Amperes per gram of an active material (including binder) is the discharge current, Δt in seconds is the discharge time, and ΔV in Volts is the voltage window from the end of the internal resistance (R) drop to the end of a discharge process.

The power density (P) is determined according to Eq. (3) [7], where V is the cell voltage and m is the total mass of both composite electrodes, i.e. $m_+ + m_-$:

$$P = \frac{V^2}{4Rm} \quad (\mathrm{W\,kg^{-1}}) \tag{3}$$

The maximum energy density (E_{max}) is obtained from the capacitance of hybrid supercapacitor (C_H):

$$E_{\max} = \frac{0.5 C_H V^2}{3600} \quad (\mathrm{Wh\,kg^{-1}}) \tag{4}$$

3. Results and discussion

3.1. Single electrode performance in a three-electrode system

The structural properties of the obtained MnO_2 were characterized using XRD, SEM, nitrogen adsorption measurements. Its electrochemical property was tested by cyclic voltammetry in a three-electrode system. As shown in Fig. 1a, the XRD pattern of MnO_2 displays clear reflections corresponding to (3 1 0), (2 1 1) and (4 4 1), which can be assigned to α-phase MnO_2 [14,26]. SEM image (Fig. 1b) shows that this MnO_2 powder consists of many agglomerated particles with primary particles sizes in the range of 20–40 nm. The nitrogen sorption isotherm and the corresponding pore size distribution (PSD) of the obtained of MnO_2 are shown in Fig. 1c. The nitrogen sorption isotherm is of type-IV characteristic with an obvious hysteretic loop at the relative pressure (p/p_0) of 0.6–0.9, indicating the presence of a mesoporous structure. The pore sizes of this sample calculated from desorption branch mainly concentrate at ca. 9.6 nm. Its BET surface area and total pore volume are 181 $m^2\,g^{-1}$ and 0.47 $cm^3\,g^{-1}$, respectively. The commercial AC used in our experiment shows type I isotherm, corresponding to

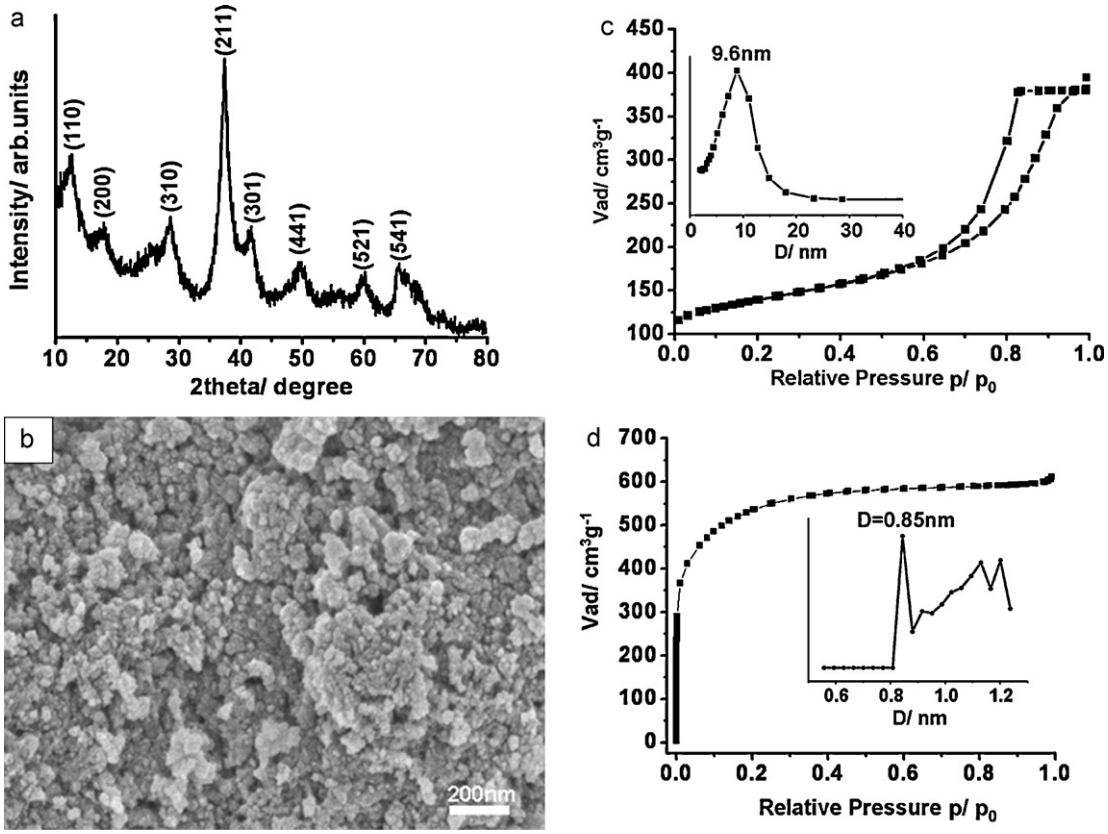

Fig. 1. XRD pattern (a) and SEM image (b) of the as-prepared MnO_2, N_2 adsorption isotherms and corresponding pore size distribution of the as-prepared MnO_2 (c) and the commercial carbon AC (d).

microporous feature. The profile of the total pore size distribution calculated according to DFT theory displays a concentrated pore size at 0.85 nm (Fig. 1d).

Fig. 2 shows the CV curves of MnO_2-based electrodes and commercial AC obtained in 0.5 M Na_2SO_4 electrolyte solution at pH 6.4 and with a scan rate of 5 mV s^{-1}. All the CVs of MnO_2-based electrodes show ideal rectangles without obvious polarizations from 0 to 0.9 V. The capacitance is mainly attributed from MnO_2 nanoparticles which work in the potential range from 0 to 0.9 V (vs. SCE) [3–6]. In contrast, AC in MnO_2&AC15 retains a dormant state and hardly offers any capacitance at this potential range. Due to an equivalent proportion of MnO_2, MnO_2&AC15 and MnO_2&AB25 exhibit approximately equivalent capacitance. MnO_2&AB10 shows a higher capacitance than MnO_2&AC15 because of a larger proportion of MnO_2. For the AC electrode, the CV profile demonstrates

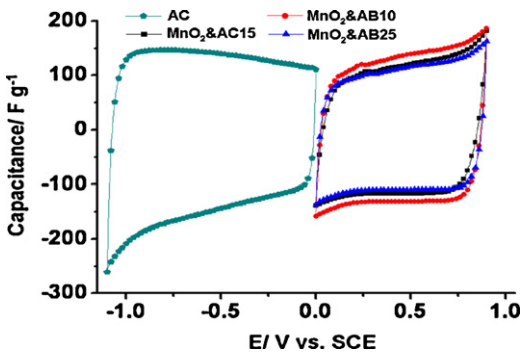

Fig. 2. Cyclic Voltamogramms (CV) of MnO_2&AC15, MnO_2&AB10, MnO_2&AB25 and activated carbon electrode obtained in 0.5 M Na_2SO_4 aqueous solution with a scan rate of 5mV s^{-1}.

an ideal double layer behavior without any noticeable redox peak from −1.1 to 0 V. The calculated specific capacitance is 160 F g^{-1} for MnO_2 and 160 F g^{-1} for AC, correspondingly (subtract the mass of binder and acetylene black). In order to exclude the possible attribution of conductive agent AB on the capacitance, a blank test of AB was primarily performed. The CV curve of AB shows a very narrow rectangle in shape (Fig. S1) and the calculated specific capacitance of AB is 3.4 F g^{-1}, which is negligible.

3.2. Hybrid characteristics in a two-electrode system

Differing from those previously reports related to asymmetric supercapacitors [4–13], the working principle of our proposed hybrid SC is illustrated in Scheme 1. In this two-electrode system, the electrochemical operating window can be divided into two distinct parts, i.e. approximate symmetric range from 0 to 1.1 V and asymmetric range from 1.1 to 2.0 V. In the potential range from 1.1 to 2.0 V, the negative electrode made from AC and the positive electrode from MnO_2 construct an asymmetric structure to supply pseudo-capacitance. Interestingly, AC in the positive electrode, owing to its moderate conductivity can be employed to partly substitute AB which usually used in the MnO_2-based positive electrode. Moreover, it also serves as the effective substance to storage charge in the voltage range of 0–1.1 V. Hence, AC in positive electrode and negative electrode forms a parallel circuit from 0 to 1.1 V. In the view of this holistic supercapacitor, a series circuit combines with two parts: one part is the parallel circuit based on ACs in the two electrodes and another part is the positive electrode of MnO_2.

The electrochemical behaviors of such hybrid SC were tested in a two-electrode glass cells. To obtain the maximum energy density [27], the mass proportion of electrode materials used is calculated by the equivalence of charge stored in each electrode in hybrid

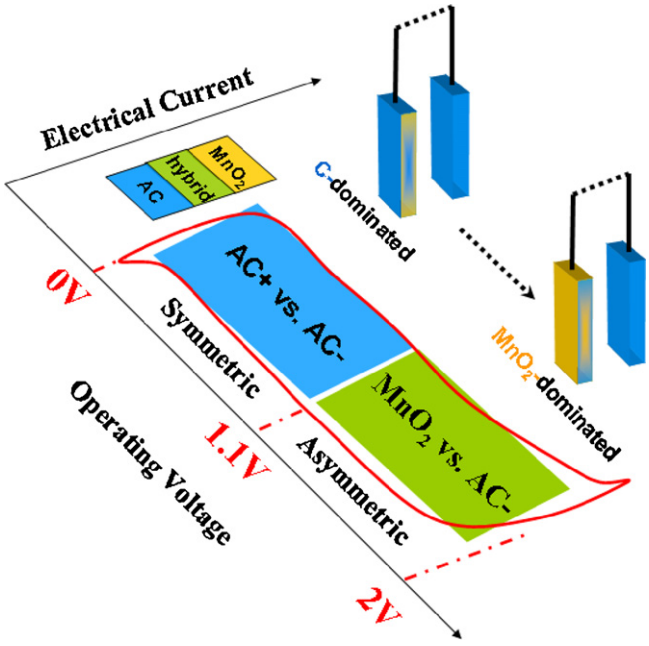

Scheme 1. Working principle diagram of an AC-MnO_2&AC hybrid supercapacitor.

capacitors:

$$\Delta E_{C-} \times C_{C-} \times m_{C-} = \Delta E_{C+} \times C_{C+} \times m_{C+} + \Delta E_{MnO_2} \times C_{MnO_2} \times m_{MnO_2} \quad (5)$$

where M_{MnO_2}, M_{C+} and M_{C-} are the mass of MnO_2 and AC in a positive electrode and mass of AC in a negative electrode, respectively; C_{MnO_2}, C_{C+} and C_{C-} are their corresponding specific capacitance tested in a three-electrode system. Herein, C_{C+} is equal to C_{C-}; ΔE_{MnO_2}, ΔE_{C+} and ΔE_{C-} are their operating voltage in Na_2SO_4 electrolyte. In the case of MnO_2 positive electrode, ΔE_{MnO_2}, value is 0.9 V, whereas ΔE_{C+} and ΔE_{C-} are identical as 1.1 V, as mentioned above. If using k to substitute C_{MnO_2}/C_C, Eq. (5) can be translated into the following equation:

$$m_{C-} = m_{C+} + 0.82km_{MnO_2} \quad (6)$$

The total mass of the positive electrode was fixed as ca. 6.5 mg. According to Eq. (6), if keeping the mass percentage of AC in the positive electrode as 15%, the calculated optimal mass of the negative electrodes was 4.7 g (see Table 2). The optimized negative (AC) and positive electrode (MnO_2&AC15) were assembled into a two-electrode hybrid SC model (AC-MnO_2&AC15). In order to demonstrate the effect of AC in positive electrode, MnO_2&AB10 and MnO_2&AB25 without AC were fabricated as positive electrodes as well, which were then constructed into hybrid SCs with AC as a negative electrode.

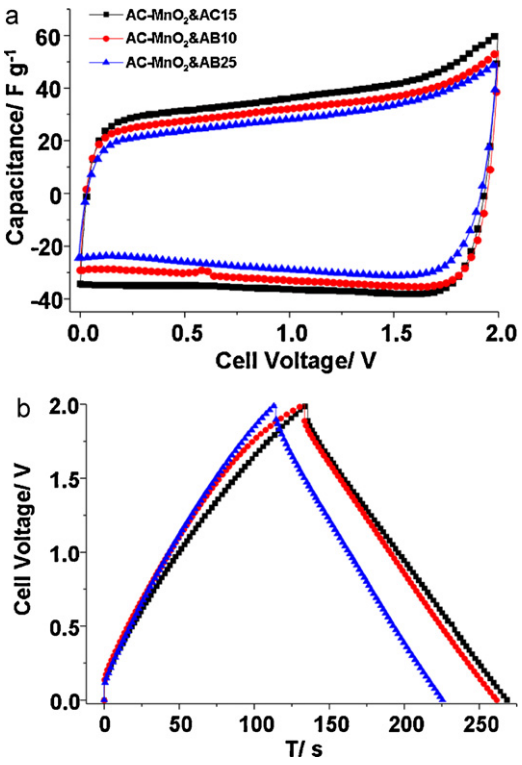

Fig. 3. (a) CVs of AC-MnO_2&AC15, AC-MnO_2&AB10, AC-MnO_2&AB25 supercapacitors at the 10th cycles and at a scan rate of 5mV s^{-1} and (b) galvanostatic charge–discharge of each supercapacitor at the 10th cycles and at a constant current of 5 mA.

Fig. 3a shows the CVs of these hybrid SCs in 0.5 M Na_2SO_4 electrolyte solution at pH 6.4 and with a scan rate of 5 mV s^{-1}. They all can be stably cycled from 0 to 2.0 V with an ideal rectangular shape, indicating a good capacitive feature. However, according to the rectangular area, the charge-storage capacity of AC-MnO_2&AC15 is obviously superior to other SCs within the voltage range of 2.0 V, reflecting a capacitance contribution from the AC in the positive electrode. Fig. 3b exhibits GC curves for these hybrid SCs at the 10th cycles and at a constant current of 5 mA. Owing to its good electrical conductivity for AC-MnO_2&AC15, the voltage adds and drops almost linearly with time increasing, exhibiting a well capacitive behavior which is analogous to that of AC-MnO_2&AB25. The coulomb efficiency of both SCs can achieve 100%. However, there is an obvious flexion in the charge branch of AC-MnO_2&AB10, indicating a significant contribution from pseudo-capacitance. The coulomb efficiency of AC-MnO_2&AB10 is remained 95% after ten cycles. Obviously, 10 wt.% of AB in the positive electrode is insufficient for achieving ideal charge–discharge behavior, and the addition of certain amount of AC in the positive electrode is an effective way to improve the conductivity. The specific capacitances of

Table 2
Data summary of the hybrid supercapacitors at the 10th cycle.

Supercapacitors	$m_{negative}$[a] (mg)	$C_{theoretic}$[b] (F g^{-1})	$C_{10cycles}$[c] (F g^{-1})	$R_{10cycles}$[d] (Ω)
AC-MnO_2&AC7	4.6	34.0	33.7	12.1
AC-MnO_2&AC15	4.7	33.6	33.2	8.41
AC-MnO_2&AC25	4.9	32.0	30.5	7.85
AC-MnO_2&AC35	5.0	29.0	27.1	8.21
AC-MnO_2&AB10	5.3	–	31.5	11.3
AC-MnO_2&AB25	4.4	–	29.6	9.61

[a] $m_{negative}$, mass of AC in negative electrode.
[b] $C_{theoretic}$, theoretical capacitance of each hybrid supercapacitor from Eq. (10).
[c] $C_{10cycles}$, capacitance of hybrid supercapacitor at the 10th cycles calculated from the discharge branch of GC curves at a constant current of 5 mA.
[d] $R_{10cycles}$, internal resistance of hybrid supercapacitor at the 10th cycles at pulse amplitude of 5 mV and pulse width 1 ms.

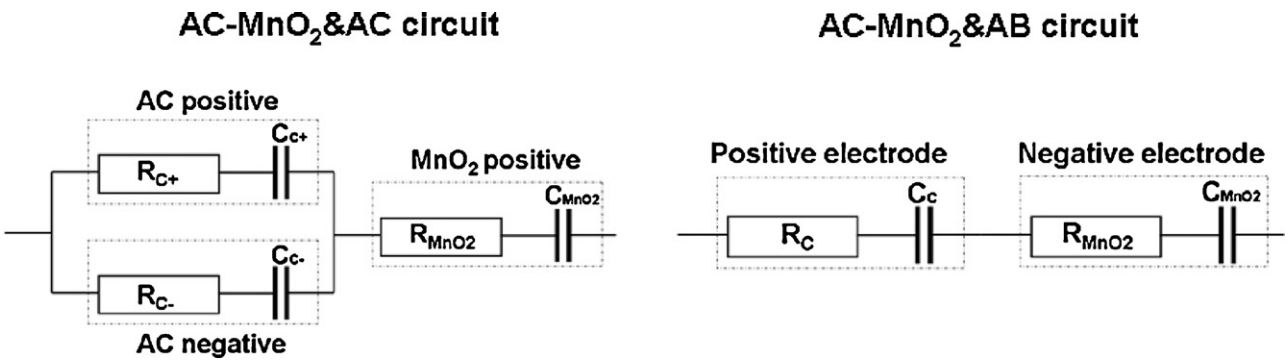

Scheme 2. Equivalent circuits of AC-MnO_2&AC and AC-MnO_2&AB supercapacitors.

the hybrid SCs were evaluated in the light of discharge branch and the results were compiled in Table 2.

The capacitance of AC-MnO_2&AC15 is 33.2 F g^{-1}, higher than that of AC-MnO_2&AB10 (31.5 F g^{-1}) and of AC-MnO_2&AB25 (29.6 F g^{-1}). Conclusively, AC used in the positive electrode can, on one hand, improves the electrical conductivity of the MnO_2 positive electrode in the voltage range of 1.1–2.0 V, while on the other hand, provides double layer capacitance in the parallel circuit from 0 to 1.1 V. Whereas, AB hardly bring any positive contribution to the charge-storage cycle, but mass increase of an electrode disc. Thus, it is not surprising that AC-MnO_2&AB10 and AC-MnO_2&AB25 show lower capacitances.

Internal resistance (R) of the SC was tested at pulse amplitude of 5 mV and pulse width 1ms. After 10 cycle tests, the internal resistances display the following order, i.e. $R_{AC-MnO_2\&AC15}(8.41\,\Omega) < R_{AC-MnO_2\&AB25}(9.61\,\Omega) < R_{AC-MnO_2\&AB10}(11.32\,\Omega)$ in sequence. Clearly, despite a higher amount of AB used, AC-MnO_2&AB25 did not exhibit a lower internal resistance. As equivalent circuits shown in Scheme 2, the resistance of AC-MnO_2&AB capacitor is $R = R_{MnO_2} + R_C$, whereas for AC-MnO_2&AC capacitor is $R = R_{MnO_2} + R_{C+}R_{C-}/(R_{C+} + R_{C-})$. On the basis of these two equations, the internal resistance of AC-MnO_2&AC15 would be lower.

It is necessary to point out, although the presence of AC in the MnO_2-based positive electrode can improve the capacitance and reduce the internal resistance, AB as conductive agent cannot be completely replaced with AC since a relatively low electrical conductivity of AC. We tried to prepare a MnO_2-based electrode (MnO_2&AC*) without using AB. The component of active substrates is $m_{MnO_2} : m_{AC} : m_{PTFE} = 70 : 25 : 5$ and the MnO_2&AC* electrode was tested in both three- and two-electrodes system as the same conditions in above. During the charge–discharge process in the high voltage, the CVs of MnO_2&AC* presented the visible polarizations in both three- and two-electrodes system (Fig. S2). The shrinkage of operating voltage is visualized for the subsistent polarization which testify the irreplaceable role of AB in MnO_2-based electrode. To enhance the electronic conductivity of MnO_2 material, the conductive agents are required in both the symmetric [18] and asymmetric [7] system. Adding in a small amount of AB, material resistance will be improved with a slight decrease of capacitance.

3.3. Functions of AC in a composite positive electrode

As indicated above, AC in the positive electrode has dual functions, i.e. as a conductive agent and as active matrix attending to the charge storage and reducing the internal resistance though the parallel connection with the AC in negative electrode. Thus, the mass proportions of AC in the positive electrode will influence the capacitance of hybrid supercapacitor [4–7].

Based on the equivalent circuits in Scheme 2, the total capacitance (F expressed in Farad) of AC-MnO_2&AC can be described as a sum of capacitance of each electrochemically active component.

$$\frac{1}{F_H} = \frac{1}{F_{C+} + F_{C-}} + \frac{1}{F_{MnO_2}} \tag{7}$$

The capacitance (F) depends on the specific capacitance (C) and the mass (m) of the active component following Eq. (8):

$$F = C \times m \tag{8}$$

In present work, the total mass of the active material is $m_H = (m_{MnO_2} + m_{C+} : m_{C-})/0.85$. Thus, the capacitance of hybrid supercapacitor (C_H) should be:

$$C_H = \frac{0.85C_{MnO_2}C_C(m_{MnO_2}m_{C+} + m_{MnO_2}m_{C-})}{(C_{MnO_2}m_{MnO_2} + C_Cm_{C+} + C_Cm_{C-})(m_{MnO_2} + m_{C+} + m_{C-})} \tag{9}$$

The relation of m_{C-}, m_{C+} and m_{MnO_2} is shown in Eq. (6). When using a to substitute m_{C+}/m_{MnO_2} and k to substitute C_{MnO_2}/C_C, Eq. (9) can be transformed as the following equation:

$$C_H = \frac{0.85C_{MnO_2}(a + 0.41k)}{(a + 0.91k)(2a + 0.82k + 1)} \tag{10}$$

When the proportion of AC in the positive electrode is fixed as certain value, the theoretical capacitance of hybrid SC can be calculated according to Eq. (10). For example, in the hybrid supercapacitor of AC-MnO_2&AC15, the proportion of AC in the positive electrode is 15 wt.%, thus the theoretical capacitance is calculated as 33.6 F g^{-1}, which is almost identical to actually measured value from GC (33.2 F g^{-1}). This confirms that the assumption of equivalent circuit of our proposed hybrid supercapacitor (AC-MnO_2&AC) is reasonable. Furthermore, by setting the ratio of specific capacitance (C_{MnO_2}/C_C) as a constant of k, the total capacitance of AC-MnO_2&AC (C_H) is thus as a function of one variable of a (representing m_{C+}/m_{MnO_2}). The maximal capacitance of AC-MnO_2&AC would be obtained when $C_H{}'_a$ equals to 0 ($C_H{}'_a$ is a derived function of C_H related to a in Eq. (10)). In the present case, the mass proportion of the conducting agent (AB) and binder (PTEF) are 10 wt.% and 5 wt.%, respectively. The optimum mass proportion of a (m_{C+}/m_{MnO_2}) can be expressed as:

$$a = 0.5k^{-1/2} - 0.41k \tag{11}$$

In our experiment, the specific capacitances of MnO_2 and AC are identical as 160 F g^{-1}, indicating k value equal to 1. The optimum mass proportion a is thus 0.9, corresponding to 7 wt.% AC in the positive electrode, and the maximum specific capacitance C_H would be 34.0 F g^{-1}.

In order to confirm the accuracy of the mathematical calculation, the positive electrode with a 7 wt.% of AC was fabricated into a hybrid supercapacitor model (AC-MnO_2&AC7). The CV curve of AC-MnO_2&AC7 was shown in Fig. 4. The measured capacitance of

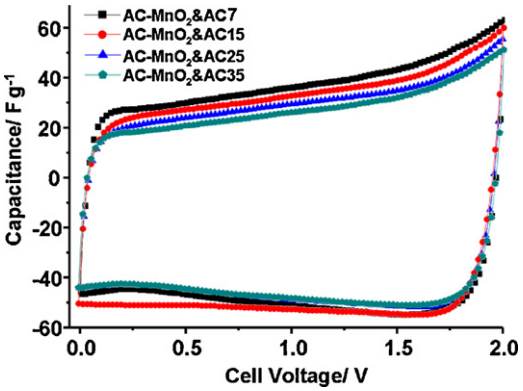

Fig. 4. CVs of AC-MnO_2&AC_x (x = 7, 15, 25, 35) tested in 0.5 M Na_2SO_4 aqueous solution at a scan rate of 5 mV s^{-1} in a two-electrode system.

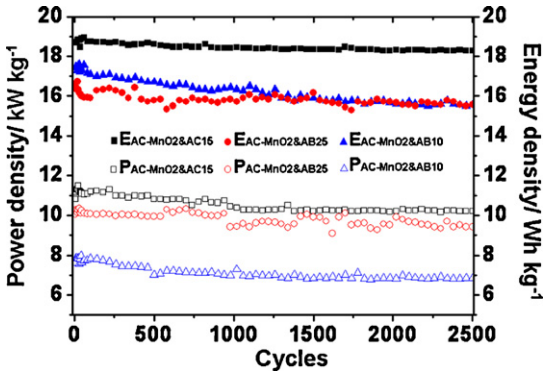

Fig. 5. Power density and maximum energy density of AC-MnO_2&AC15, AC-MnO_2&AB10, AC-MnO_2&AB25 supercapacitors at a constant charge–discharge current of 10 mA between 0 V and 2 V.

AC-MnO_2&AC7 is 33.7 F g^{-1} which is close to the theoretical value of 34.0 F g^{-1}, demonstrating that our proposed equation is correct and can be applied for directing the fabrication of hybrid supercapacitors using different electrode materials. It need to be pointed out that the measured internal resistance of AC-MnO_2&AC7 is 12.1 Ω, indicating such less AC (7 wt.%) is insufficient to reduce the internal resistance according to the equivalent circuits shown in Scheme 2. When the mass proportion of AC in a positive electrode slightly increased to 15%, the measured capacitance of AC-MnO_2&AC15 is 33.2 F g^{-1} and the internal resistance is 8.41 Ω. Therefore, from the viewpoint of simultaneously achieving high energy density and power density, the capacitance and internal resistance should be integrated.

For comparison, hybrid supercapacitors containing 25 wt.% and 35 wt.% of AC in positive electrodes were also constructed. As shown in Fig. 4, due to the deviation from the optimum mass proportion of AC (7 wt.%), a downtrend of capacitance is observed along with the increasing mass proportion of AC in a positive electrode. However, with increase of AC in a positive electrode, the measured internal resistances of AC-MnO_2&AC25 and AC-MnO_2&AC35 are, as expected, reduced to 7.85 Ω and 8.21 Ω, respectively. This indicates the equivalent circuits shown in Scheme 2 are correct. Therefore, the mass proportion of AC in a positive electrode of a hybrid supercapacitor should be kept a suitable value in terms of simultaneously achieving a high power density and energy density. In our case, AC-MnO_2&AC15 supercapacitor with addition of 15 wt.% AC in the positive electrode was demonstrated to be the optimized condition.

3.4. Cyclical stability measurement

The cycling stability of the AC-MnO_2&AC15 hybrid supercapacitor during a charge–discharge process was further investigated over 2500 cycles in the voltage range from 0 to 2.0 V with a constant current of 10 mA in a two-electrode glass cell. The internal resistance was tested after per 50 cycles at pulse amplitude of 5 mV and a pulse width 1 ms. For comparison, the cycling stability of AC-MnO_2&AB25 and AC-MnO_2&AB10 hybrid supercapacitors without addition of AC in the positive electrodes were also tested under the same conditions. As reflected in Fig. 5, the AC-MnO_2&AC15 hybrid supercapacitor retains good charge–discharge performance, and its coulomb efficiency after 2500th cycles is 99%. A slight loss (≈4%) in capacitance and a slight increase (≈8%) in internal resistance were observed for AC-MnO_2&AC15 supercapacitor after 2500 cycles. The energy density and power density determined by Eqs. (3) and (4) after 2500 cycles are 18.2 Wh kg^{-1} and 10.1 kW kg^{-1}, respectively. Although AC-MnO_2&AB25 retained a stable state (~5% loss in capacitance and ~7% rise in internal resistance) during the 2500 tests, the low energy density is a remarkable drawback. For AC-MnO_2&AB10 supercapacitor, a capacitance drop of ~11% after 2500 cycles was observed, which is mainly attributed to the continuous growth of the internal resistance.

4. Conclusions

A novel strategy for the fabrication of a hybrid supercapcitor consisting of a composite-based positive electrode and a carbon-based negative electrode has been established. Due to the parallel connection of AC in the positive and negative electrodes, an increase in specific capacitance and a decrease in internal resistance of a hybrid supercapacitor have been observed. To maximize the capacitance of a hybrid supercapacitor, the mass proportion of the active substances in a positive electrode needs to be optimized, which can be done followed a theoretical calculation. In the present work, under the consideration of achieving high power density and energy density, the optimal mass proportion of AC in a positive electrode was set as 15%, a good cycle performance of AC-MnO_2&AC15 has been demonstrated. To the best of our knowledge, this is the firstly highlight of the dual functions of AC in positive electrode. It thus may provide a working principle for developing high energy density and environmentally friendly supercapacitor systems.

Acknowledgment

We sincerely appreciate the financial support by Program for New Century Excellent Talents in University of China (NCET-08-0075).

Appendix A. Supplementary data

Supplementary data associated with this article can be found, in the online version, at doi:10.1016/j.jpowsour.2010.12.056.

References

[1] J.R. Miller, P. Simon, Science 321 (2008) 651–652.
[2] P. Simon, Y. Gogotsi, Nat. Mater. 7 (2008) 845–854.
[3] M.S. Hong, S.H. Lee, S.W. Kim, Electrochem. Solid-State Lett. 5 (2002) A227–A230.
[4] V. Khomenko, E. Raymundo-Piñero, F. Béguin, J. Power Sources 153 (2006) 183–190.
[5] V. Khomenko, E. Raymundo-piñero1, E. Frackowiak, F. Béguin, Appl. Phys. A 82 (2006) 567–573.
[6] T. Brousse, M. Toupin, D. Bélanger, J. Electrochem. Soc. 151 (2004) A614–A622.
[7] T. Brousse, P. Taberna, O. Crosnier, R. Dugas, P. Guillemet, Y. Scudeller, Y. Zhou, F. Favier, D. Bélanger, P. Simon, J. Power Sources 173 (2007) 633–641.
[8] Q. Qu, Y. Shi, S. Tian, Y.H. Chen, Y.P. Wu, R. Holze, J. Power Sources 194 (2009) 1222–1225.
[9] Q. Qu, L. Li, S. Tian, W. Guo, Y. Wu, R. Holze, J. Power Sources 195 (2010) 2789–2794.

[10] D.W. Wang, H.T. Fang, F. Li, Z.G. Chen, Q.S. Zhong, G.Q. Lu, H.M. Cheng, Adv. Funct. Mater. 18 (2008) 3787–3793.
[11] Y.G. Wang, Z.D. Wang, Y.Y. Xia, Electrochim. Acta 50 (2005) 5641–5646.
[12] Q.T. Qu, Y. Shi, L.L. Li, W.L. Guo, Y.P. Wu, H.P. Zhang, S.Y. Guan, R. Holze, Electrochem. Commun. 11 (2009) 1325–1328.
[13] T. Brousse, R. Marchand, P.L. Taberna, P. Simon, J. Power Sources 158 (2006) 571–577.
[14] H.Y. Lee, J.B. Goodenough, J. Solid State Chem. 144 (1999) 220–223.
[15] S.B. Ma, K.W. Nam, W.S. Yoon, J. Power Sources 178 (2008) 483–489.
[16] C.Y. Lee, H.M. Tsai, H.J. Chuang, J. Electrochem. Soc. 152 (2005) A716–A720.
[17] H. Zhang, W.F. Zhang, J. Cheng, G.P. Cao, Y.S. Yang, Solid State Ionics 179 (2008) 1946–1950.
[18] P.L. Taberna, C. Portet, P. Simon, Appl. Phys. A 82 (2006) 639–646.
[19] G.X. Wang, B.L. Zhang, Z.L. Yu, M.Z. Qu, Solid State Ionics 176 (2005) 1169–1174.
[20] V. Subramanian, H. Zhu, B. Wei, Electrochem. Commun. 8 (2006) 827–832.
[21] Y.T. Wu, C.C. Hu, J. Electrochem. Soc. 151 (2004) A2060–A2066.
[22] A.E. Fischer, K.A. Pettigrew, D.R. Rolison, R.M. Stroud, J.W. Long, Nano Lett. 7 (2007) 281–286.
[23] C. Liu, F. Li, L.P. Ma, H.M. Cheng, Adv. Mater. 22 (2010) E1–E35.
[24] D.W. Wang, F. Li, M. Liu, G.Q. Lu, H.M. Cheng, Angew. Chem. Int. Ed. 47 (2008) 373–376.
[25] Y. Wang, C.Y. Foo, T.K. Hoo, M. Ng, J. Lin, Chem. Eur. J. 16 (2010) 3598–3603.
[26] S. Devaraj, N. Munichandraiah, J. Phys. Chem. C 112 (2008) 4406–4417.
[27] X. Wang, J.P. Zheng, J. Electrochem. Soc. 151 (2004) A1683–A1689.